IEEE Access
Multidisciplinary | Rapid Review | Open Access Journal

Received 9 February 2024, accepted 22 February 2024, date of publication 26 February 2024, date of current version 5 March 2024.

*Digital Object Identifier 10.1109/ACCESS.2024.3370560*

RESEARCH ARTICLE

# Improving Output Performance of the Ultrasonic Multicell Piezoelectric Motor by Development the Multi-Rotor Structure

**ROLAND RYNDZIONEK, (Senior Member, IEEE)**
Faculty of Electrical and Control Engineering, Gdańsk University of Technology, 80-233 Gdańsk, Poland
e-mail: roland.ryndzionek@pg.edu.pl

**ABSTRACT** In recent years, many researches have been carried out on piezoelectric multi-rotor structures. This paper describes the analysis, development and experimental process of an ultrasonic multi-cell piezoelectric motor using a multi-rotor structure. In this design, three independent cells have been integrated into a mechatronic system. Analytical model and finite element method are used for modal and dynamic analysis of the proposed motor. The multicell motor prototype has been manufactured and tested in the laboratory. Finally, the results of analytical, simulations and experimental investigation have been compared. The compared results are in satisfactory agreement. The measured parameters were: resonance frequency characteristics, mechanical characteristics of the single actuator and the complete assembled motor. The maximum speed and load of the motor have been determined. The maximum speed of 512 rpm was obtained with a voltage of 86 Vrms and the maximum stall torque was 120 mNm. Finally, the multi-rotor structure was compared with other rotary ultrasonic structures.

**INDEX TERMS** Piezoelectric actuator, piezoelectric ultrasonic motor, piezoelectricity, travelling wave motor, rotary motor.

## I. INTRODUCTION

The research and design of piezoelectric transducers, motors and sensors is a complex and labour intensive process [1], [2], [3], [4]. The construction of a prototype piezoelectric motor that meets the assumed input parameters and output characteristics requires the development and application of validated test methods. A variety of methods are available in the literature for the determination and verification of these parameters and characteristics. Unfortunately, piezoelectric motors are frequently described in a simplified manner, limiting the ability to compare their parameters and characteristics. Furthermore, the presentation and justification of results when verifying piezoelectric motors often fall short due to the diverse nature of their structures.

The strongly coupled elastic and electrical equations and the coupled constitutive relations are the main difficulties in the theory/modelling of piezoelectric motors or actuators [5], [6]. In addition, the modelling, structural and technological problems of piezoelectric structures are related to the constitutive parameters of the piezoelectric materials used in their construction. It should be noted that, despite these problems, progress has been made in the development of modelling methods [7]. Moreover, the development of ultrasonic piezoelectric actuators and motors is made possible by ongoing research into electro-active materials, particularly new ceramic materials and polymers with high 'power density' and low loss [8], [9]. The popular piezoelectric materials are ferroelectric polycrystalline ceramics such as barium titanate (BaTiO3) and lead zirconate titanate (PZT). The development of this technology is relevant to engineering fields such as automotive, aerospace, precision manufacturing, optical scanning, biotechnology and medicine, and energy harvesting [10], [11], [12], [13], [14].

Compared to conventional electromagnetic structures, the field of piezoelectric motors is relatively new. The most common classification of the piezoelectic ultrasonic motors in the literature is based on individual vibration types [15],

The associate editor coordinating the review of this manuscript and approving it for publication was Riccardo Carotenuto.

[16]. In addition, it is often stated that piezoelectric motors have simpler and less complex control systems than electromagnetic motors because they do not require sophisticated control algorithms [17]. Piezoelectric transducers and motors cannot replace electric motors on a large scale due to their performance characteristics (e.g. low efficiency) [18], [19]. However, there are applications where they have a certain advantages - operation in a strong magnetic field and resistance to interference, or complex mechatronic systems that require movement in several directions (reducing the mass and volume of a given system by replacing several linear motors with a single design) [5], [20]. The main challenges at present are the development of new, more reliable structures and methods for evaluating piezoelectric motors, and the development of new strategies for driving piezoelectric systems to achieve higher efficiencies. Another important issue is the efficient removal of the heat generated by friction, which ultimately reduces efficiency.

This paper describes the use of research methods: analytical, simulation and experimental studies to developed and evaluation the prototype structure. The main contribution has been to demonstrate that the use of a multi-rotor structure can improve the output speed and the torque. Moreover, in the multicell piezoelectric motor (MPM) structure, the input and output characteristics must be related to the mass/volume of the motor.

The structure of the developed motor is introduced, and its principle of operation is described in section II. The analytical and FEM method of new MPM is presented in section III. Furthermore, the simulation results and the analytical calculation are compared with and verified by experiment results in section IV. Finally, the main conclusions are elaborated.

## II. MULTI-ROTOR PIEZOELECTRIC MOTOR DESCRIPTION

This paper proposes a multi-rotor driven resonant motor. In general, a piezoelectric motor consists of a few basic elements: stator, piezoelectric ceramics, rotor, shaft (Fig. 1).

The mechanical structure operates in the ultrasonic resonance frequency range, generating micro-vibrations. A wave (running or standing) can be generated from these vibrations. This is due to the use of the inverse piezoelectric phenomenon - the generation of vibrations in a piezoelectric material by the application of an electrical voltage. Hence these motors are referred to as ultrasonic running wave or standing wave motors.

This structure is the result of experience from previous research work published in [21], [22], and [23]. The motor presented in this article is free from the drawbacks of its predecessors like: assembly problems, resonance frequeny differences, parasitic resonances' influence, the rotor acting on three separate actuators reduces the overall efficiency due to the loss of contact.

The MPM structure consist of three pairs of actuators and sets of piezoelectric ceramics (stator), three pairs of rotors and shaft (Fig. 2). Three pairs of actuators are the minimum

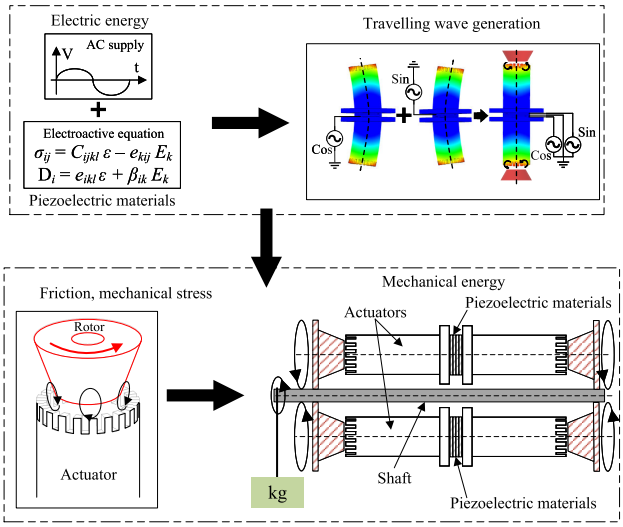


**FIGURE 1. Simplified diagram of the operation and energy conversion process in a multicell piezoelectric motor.**

number to ensure the stability of the structure. In order to achieve a relatively high electromechanical efficiency and the desired mechanical properties, a screw-clamp structure was adopted to induce strong vibrations and exploit the $d_{33}$ modes of the piezoceramics. It is extremely important to apply a counter-mass to the two bending modes using the first order vibrations of the piezo-ceramics (the so-called bending mode). Such a mode of operation can be achieved by exciting the piezoceramic plates with two voltage signals that are exactly 90° out of phase with each other. In the literature such a mode of operation is referred to as the 'dual-phase excitation method' [24], [25]. The piezoelectric ceramic generates a travelling wave that drives the stator. This creates friction with the rotor in the actual operation of an ultrasonic motor.

## III. PROTOTYPE DEVELOPMENT

Modelling piezoelectric motors is similar to modelling electrical machines and can be done in two ways. Based on field dependencies [26] and based on simplified equivalent circuit methods [27], [28]. It should be noted that equivalent circuit modelling is much more common - more widely used. However, there is no consistent transition from field modelling to circuit modelling.

A number of preliminary conditions and design assumptions have been considered in this research:

- resonance frequency above 20 kHz,
- diameter of a single counter-mass element 12.5 mm (due to the piezoelectric ceramics diameter),
- significantly improved speed compared with previous MPM structures,
- modular structure with reduce overall mass of the motor.
- actuator material: aluminium.

The single actuator structure has been presented in the Fig. 3. The diameter of the actuator and the piezoelectric ceramic is the same - 12.5 mm. The number of drive teeth

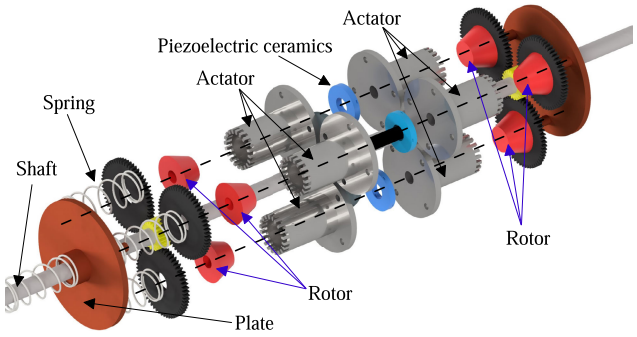


**FIGURE 2.** Three-dimensional structure of the multicell piezoelectric motor structure with multi rotors.

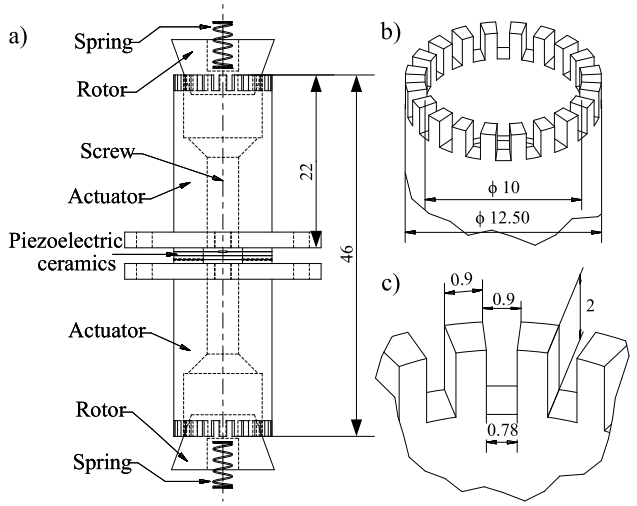


**FIGURE 3.** Single actuator structure: a) the cross-section of the single actuator, b) the isometric view of the actuator and rotor contact surface, c) the dimension of the teeth. All dimensions are in milimiters.

**TABLE 1.** Properties of the materials used in MPM: piezoelectric ceramic NCE40 and aluminium.

| Symbol | Quantity | Value |
|---|---|---|
| $\varepsilon_{33}^T/\varepsilon_0$ | Relative dielectric constant | 1250 |
| $k_{31}$ | Electromech. coupling factors | 0.34 |
| $k_{33}$ | | 0.70 |
| $k_{31}$ | | 0.50 |
| $d_{31}$ | Piezoelectric charge constant [10-12 C/N] | -140 |
| $d_{33}$ | | -320 |
| $Q_M$ | Quality factor | 700 |
| $\rho$ | Density PZT NCE40 [kg/$m^3$] | 7750 |
| $E$ | Aluminium Young's modulus [$10^9$ Pa] | 69 |
| $\rho$ | Aluminium density [kg/$m^3$] | 2770 |
| $\nu$ | Aluminium Poisson's ratio [-] | 0.35 |

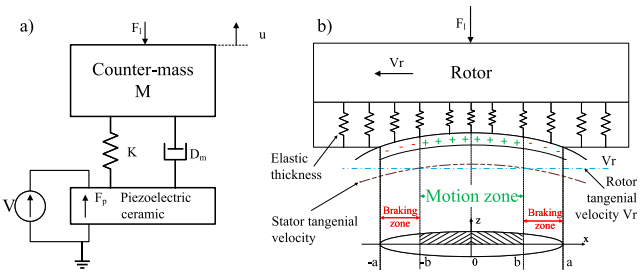


**FIGURE 4.** a) The simplest model of an elementary piezoceramic resonantsystem, b) the tangential velocity and friction distribution.

at the end of the actuator is 20 and the width and height are 0.9 mm and 2 mm respectively. The rotor has a trapezoidal cross-section with a 60° angle of inclination. This angle allows a very good fit and centring in the inner part of each actuator (The previous MPM prototype had an inclination angle of 45°, which caused the rotor to move excessively). The material of the actuator is aluminium, the rotor is stainless steel and piezoelectric ceramics are NCE40 from Noliac. The properties of the ceramics have been presented in Table 1.

### A. ANALYTICAL MODELLING

The simplest model of an elementary piezoceramic resonant system (Fig. 4a) consists of a few basic elements: piezoceramics denoted as piezoelectric material (e.g. PZT), a countermass denoted as $M$, a helical spring constant denoted as $K$, a damping coefficient denoted as $D_M$, a voltage source denoted as $V$ and a load denoted as $F_l$ [29]. Its kinetic energy can be assumed to be negligible, since the mass of the piezoelectric ceramic is negligibly small relative to the mass of $M$. The piezoelectric active element acts as a mechanical spring and the system's oscillation amplitude is at its maximum at resonant frequency [30], [31]. The piezoelectric material generates a voltage that is proportional to the applied mechanical force. When the system is excited to its resonant frequency, mechanical and electrical energy is transferred between the active element and the counter mass, increasing the amplitude of oscillation [32].

The co-directionality of the electric field and the principal displacement of the rotor are assumed in the piezoelectric motor considered in this paper. A three-turn system has been implemented in the model. The power system consists of two voltage sources with 90° electrical degrees shift, piezoelectric ceramics and a rotor. The motor has a two-component displacement field in the rotor zone - tangential and axial - and a tangential electric field (Fig. 4b). The area between the points *"b"* corresponds to the rotor speed $Vr$. The directional motion of the rotor is determined by the negative positive values. Negative if $V<Vr$ and positive if $V>Vr$. Appropriate excitation of the piezoelectric ceramics produces two perpendicularly intersecting modes of counter-mass vibration. These are excited by the inverse piezoelectric effect of the piezoelectric elements.

The oscillations of the counter-mass $U$, in the $x$ and $y$ axes, can be written using the following formula:

$$U_x = U_0 cos(\omega t)$$
$$U_y = U_0 sin(\omega t) \quad (1)$$

Counter-mass oscillations after transformation with trigonometric identities:

$$U_\tau = U_0 cos(\omega t - \varphi)$$
$$U_r = U_0 sin(\omega t - \varphi) \quad (2)$$

By summing and substituting, the equation for a travelling wave at $u$ is obtained:

$$u = u_x + u_y = -rcos\varphi U_0' cos(\omega t) - rsin\varphi U_0' sin(\omega t)$$
$$= -rU_0' cos\varphi(\omega t - \tau) \quad (3)$$

$$\left\{ \begin{array}{l} U_\tau = U_0 cos(\omega t - \varphi) \\ U_r = U_0 sin(\omega t - \varphi) \\ u = -rU_0' cos\varphi(\omega t - \tau) \end{array} \right\} \quad (4)$$

where $r$ is radius of the cross section single actuator. The diameter of the single actuator is 12.5 mm, thus in this case $r$ is equal to 6.25 mm.

The model allows the determination of the maximum displacement of the counter-mass as a function of the applied supply voltage and the contact force between the rotor and the counter-mass. These voltages can be calculated using the Hertz theory and associated with a constant coefficient of friction between the stator and the rotor. The influence of the vibrations generated by two sinusoidal signals with a similar resonant frequency and an additional bending mode of third order is shown. The equation of motion is described by the formula:

$$\begin{bmatrix} M_y & 0 \\ 0 & M_z \end{bmatrix} \begin{bmatrix} \ddot{u}_r \\ \ddot{u}_t \end{bmatrix} + \begin{bmatrix} D_y & 0 \\ 0 & D_z \end{bmatrix} \begin{bmatrix} \dot{u}_r \\ \dot{u}_t \end{bmatrix} + \begin{bmatrix} K_y & 0 \\ 0 & K_z \end{bmatrix} \begin{bmatrix} u_r \\ u_t \end{bmatrix} = \begin{bmatrix} F_y \\ F_z \end{bmatrix} \quad (5)$$

In this case, the amplitudes of the tangential and longitudinal vibrations are defined as $U_t$ and $U_r$ respectively. The relationship between the output vibration $U_r$ and the applied voltage $U_0$ is:

$$\frac{U_r}{U_0} = \frac{n \cdot d_{33} \cdot K_y \cdot K_z}{(R_c D_z + 1)[(M_y + M_z)s^2 + (D_y + D_z)s + (K_y + K_z)]} \quad (6)$$

where: $n$ is the number of piezoelectric ceramics, $d_{33}$ is the piezoelectric coefficient, $R_c$ is the voltage supply resistance.

The tangential velocity and maximum rotor speed has been calculated from [33] and [34]:

$$\Omega_{max} = U_\tau = U_0 \omega cos(\frac{x}{r}) \quad (7)$$

The maximum theoretical torque in the single actuator has been assumed from:

$$T_{max} = 2\mu r F_{load} \quad (8)$$

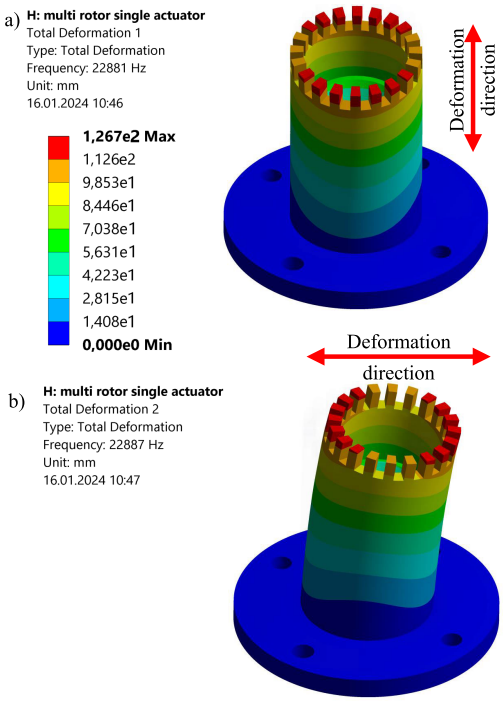


**FIGURE 5.** The results of vibration modes of variable-natural-frequency a) first bending vibration mode and b) second bending vibration mode in the single actuator of the MPM.

The load applied to the motor is determined by the specified load $F_{load}$ and the calculated steady-state motor speed from (7). The average output power is:

$$P_{avg} = F_{load} \cdot \Omega_{max} \quad (9)$$

In the following chapters, the analytical model calculations are compared with simulations and experimental results.

### B. FEM ANALYSIS

The Finite Element Method (FEM) is a widely used technique for the development of piezoelectric actuators. In efforts to enhance vibration generation, a detailed analysis of the actuator's shape and configuration was conducted.

To determine the first mode of vibration of the actuator and assess its movement performance, a series of simulations were executed using the ANSYS Workbench. The analysis focused on the dimensions of the teeth and the height of a single actuator. The impact of length on the resonant frequency and the magnitude of vibrations generated at resonant frequencies was investigated through FEM simulations conducted on the actuator model (Fig. 5). The mesh is composed of 30,000 elements, which were achieved through a software-controlled adaptive refinement process. The actuator is fixed by constraints on the bottom side.

The modal analysis shows several resonance frequencies in the range of 10 kHz to 50kHz. However, in the case of MPM, only a few of these are useful for the generation of torque and speed. The first- and second order resonant frequencies are 22.881 kHz and 22.887 kHz, respectively. It is

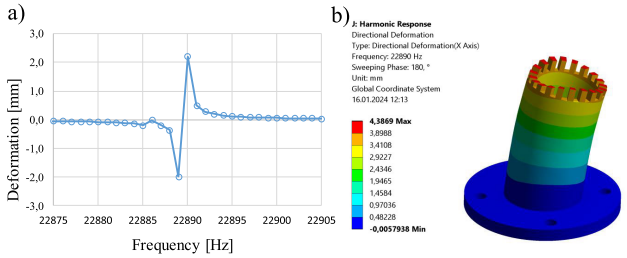


**FIGURE 6.** The results of harmonic response simulation a) amplitude vs frequency b) maximum directional deformation.

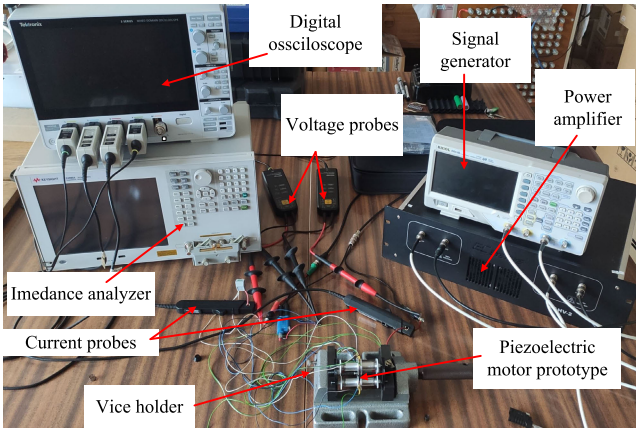


**FIGURE 7.** Laboratory test bench for experimental setup of MPM with multi-rotor structure.

important that the two bending modes are very close to each other. This enables the generation of travelling waves.

The harmonic response analysis has been carried out. This analysis is required to determine the steady-state response of structure to loads that vary sinusoidal. A point on the contact surface of one of the drive teeth is selected as the calculation point. The results are in agreement with the predicted resonant frequency diagram from the measurement. The highest displacements are in 22.887-22.890 kHz.

## IV. EXPERIMENTAL TESTS

The piezoelectric motor prototype has been manufactured. The single actuator has been precisely maachined by a CNC machine. The detailed dimensions including driving teeth are presented in Fig. 3b and Fig. 3c. The assembly element connects three individual actuators, a pressure plate, and rings. The mechanical gears in the rotor and shaft were extracted from a planetary gearbox. The rotor gear has 38 teeth, and the shaft gears have 26 teeth with a pitch rate of 0.5. All gear wheels are made of epoxy resin to ensure they remain lightweight and robust throughout their lifespan.

The laboratory test bench for experimental setup has been presented in Fig. 7. Motor assembly has been presented in Fig. 8. The power supply setup include: a high-voltage linear amplifier PAHV-2 which was controlled by a Rigol DG4102 signal generator, digital oscilloscope Tektronix

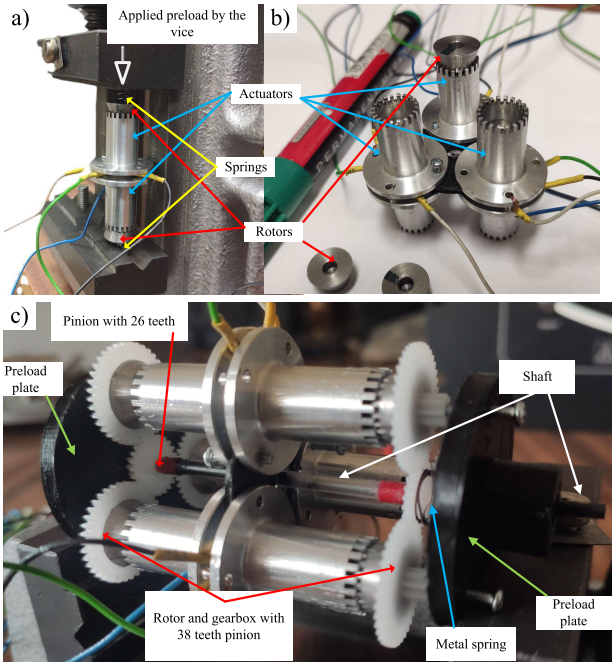


**FIGURE 8.** a) Single actuator assembly under the preload test, b) stator structure with three actuators integration, c) full motor assembly with multi rotor structure.

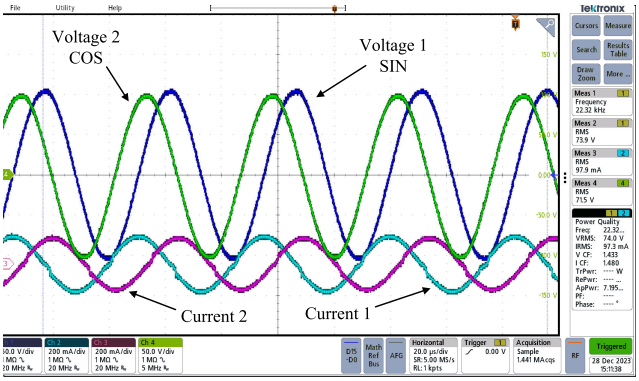


**FIGURE 9.** Supply voltage and current waveforms of the MPM.

MDO34 with two voltage (model THDP 0200) and current (model TCP0020) probes. The speed was measured using laser non-contact velocimeter (Digital Laser Tachometer DT-205LR). With this setup it was possible to control voltage frequency as close to the frequency of mechanical resonance.

The voltage of the power supply is limited to around 80Vrms or 225 Vp-p (Fig. 9). The output signal becomes distorted above this value due to the capacitive nature of the motor.

In the test bench, the three actuators are connected in parallel to a single channel of the power amplifier. The voltage and current are measured at the output terminals of the power amplifier.

### A. RESONANCE FREQUENCIES

Experimental analysis started by measuring the resonant frequencies of all three actuators using the Keysight vE4990A

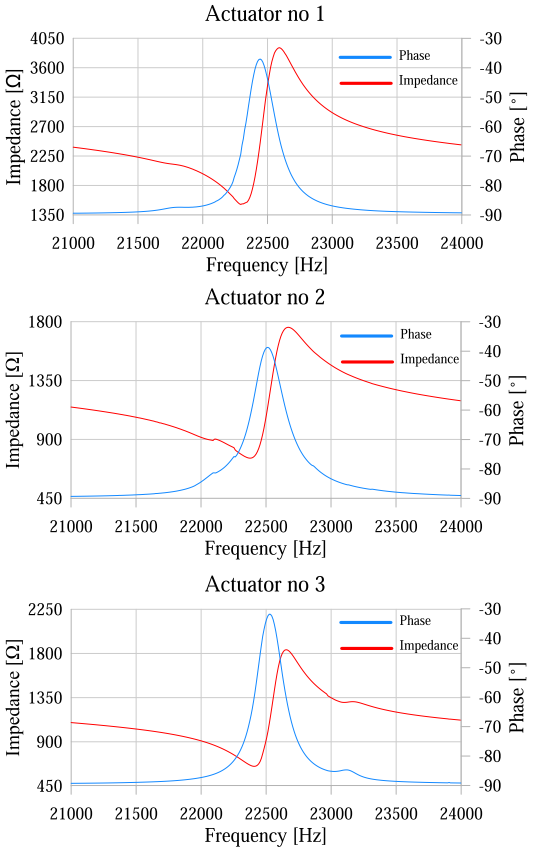


**FIGURE 10.** Results of the resonance frequency measurements for each actuator in prototype where the red line is impedance and the blue line is phase.

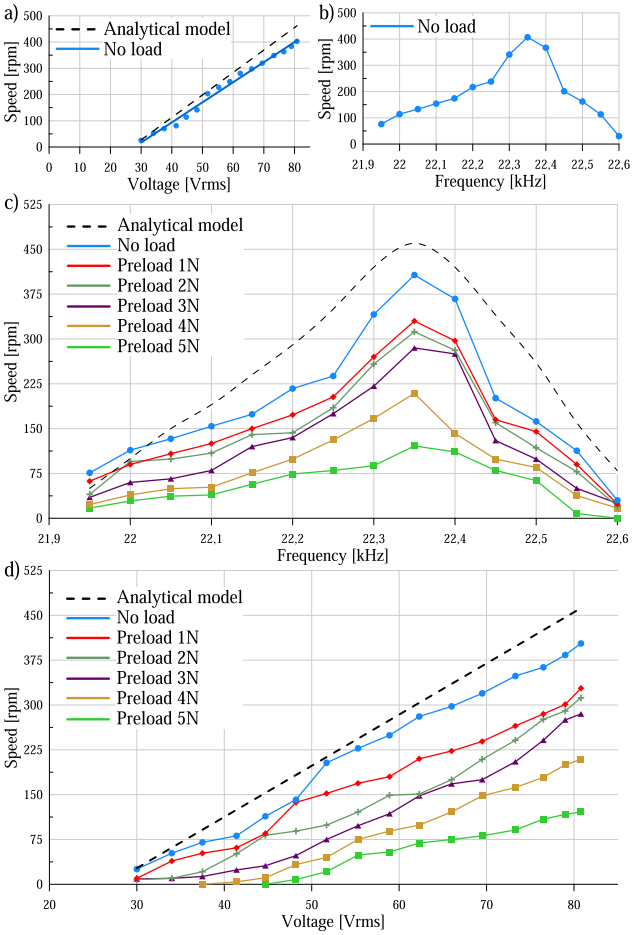


**FIGURE 11.** Experimental anaysis of the single actuator a) no-load rotor speed versus voltage, b) no load rotor speed versus frequency, c) speed vs frequency in terms of different preload, d) speed vs supply voltage in terms of different preload.

impedance analyser. Each actuator has been measured individually. The resonance frequencies test values are 22.32 kHz, 22.37 kHz, 22.38 kHz for Actuator no 1, no 2, no 3, respectively (Fig. 10). The measurements shows good agreements comparing with the analytical calculation (22.53 kHz) and FEA simulations (22.83 kHz). The difference is due to the tightening force of the screw on the two actuators. The tightening force could be increased to achieve better matching between measurement and simulation. However, it is possible to damage the prototype.

### *B. TEST PLATFORM*

Firstly, the tests have been done on the single actuator and two rotors placed in vice hanlde (Fig. 8a). The vice handle with laboratory force measuring scales allows the load to be varied precisely. The tests were carried out in a variety of scenarios: no load speed test for frequency and voltage change, speed vs frequency test under different preload (Fig. 11). The experimental results have been compared with analytical calculation from Section IIIA. Figure 11a shows the speed dependence in terms of voltage variation. It has a linear voltage characteristic which is in agreement with the analytical calculation. The maximum no-load speeds are 407 rpm and 460 rpm, measured and calculated respectively. In Fig. 11b the speed dependence in terms of frequency variation has been investigated. The maximum speed corresponds to the resonance frequency measured in Fig. 10 - 22.36 kHz. In Fig. 11c and Fig. 11d the differential preloads were applied using a vice. The resonant frequency or voltage variation was applied to ceramic. As expected, higher preload results in lower speed.

Secondly, the tests were carried out with the complete assembly (three actuators, gears, rotors and shaft). The full MPM protytype has been presented in the Fig. 8c. The gear ratio between the rotor and the shaft is 38 teeth to 26 teeth, giving a ratio of approximately 1.5. The no-load test has been presented in the Fig. 12a and b. The maximum theoretical speed, calculated on the basis of previous tests, should be 600 rpm or more. However, the maximum measured shaft speed was 512 rpm. This is due to the fact that the six rotors do not operate with sufficient speed and torque and are not in equilibrium. Nevertheless, the characteristics obtained are in line with assumptions and previous measurements. As expected, the no-load tests show a linear relationship

**TABLE 2. Comparison of piezoelectric rotary ultrasonic motors described in literature.**

| Parameter | proposed MPM | Deen Bai [35] | Yang Lin [36] | Ye Chen [37] | Lang [38] | Lu [39] | Iula [40] |
|---|---|---|---|---|---|---|---|
| Speed (rpm) | 512 | 350 | 48 | 441 | 99 | 110 | 116 |
| Torque (mNm) | 120 | 72 | 200 | 1 | 143 | 3 | 940 |
| Res. freq. (kHz) | 22.35 | 20.86 | 38.12 | 22.26 | 45.844 | 62.56 | 23.6 |
| Voltage (Vp-p) | 235 | 300 | 200 | 300 | 440 | 150 | 240 |
| Rotors | 6 | 2 | 1 | 1 | 1 | 2 | 2 |
| Structure | symmetrical | symmetrical | non-sym | non-sym | non-sym | symmetrical | symmetrical |

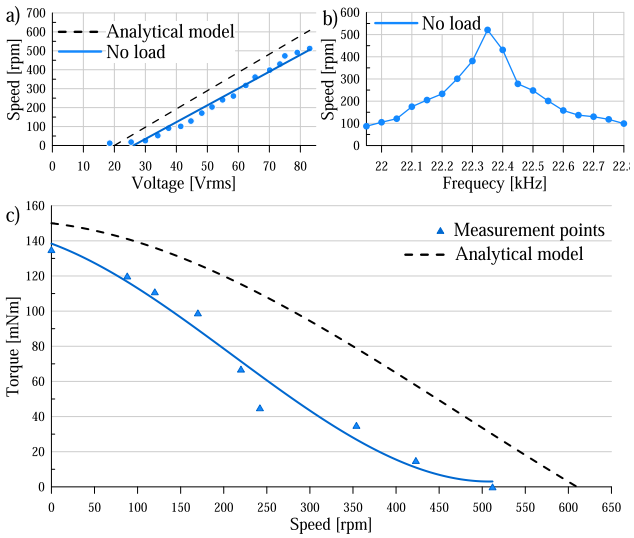


**FIGURE 12. Experimental anaysis of the full assembly structure a) no-load shaft speed versus voltage, b) no load shaft speed versus frequency, c) shaft under load - torque versus speed characteristic.**

between shaft speed and voltage. In contrast, the shaft speed-frequency characteristic is symmetrical and dropping quickly outside the resonance.

Finally, the test under load was carried out. A weight was attached to the motor shaft using a piece of wire. The load mass was determined using an electronic balance. The same set-up as described in [23]. This makes the results comparable and results from both prototypes can be compared directly. With the power supply limitations listed in the previous paragraphs, the measured blocking torque was 0.12 Nm and maximum speed of 512 rpm. The measured points and the plotted characteristics have a shape that is close to the theoretical one.

The discrepancies between the theoretical characteristics and the measurements are a result of the simplifications made in the analytical model. The model assumes perfect contact between the rotor and stator, as well as between the stator and piezoelectric ceramic, and negligible temperature effects. However, the discrepancies are not significant. It should be noted that the curves tend to be similar.

The comparisons between the proposed motor and other ultrasonic structures are presented in Tab. 2. The proposed

**TABLE 3. Comparison of MPMs - Ryndzionek previous [23] and proposed multi-rotor MPM.**

| Symbol | MPM [23] | multi-rotor MPM |
|---|---|---|
| Actuator assembly | complicated | easy |
| Full motor assembly | average | quite challenging |
| Res. freq. alignment | difficult | simplified |
| Parasitic resonances | yes | reduced |
| Max noload speed | 40 rpm | 512 rpm shaft |
| Max blocking torque | 68 mNm | 120 mNm |
| Heat generation | rapid heat-up | less heat |
| Power-weight ratio | 5.33 W/kg | 15.79 W/kg |
| Max torque-weight ratio | 0.23 Nm/kg | 0.48 Nm/kg |

MPM motor has the highest maximum no-load speed among the motors to be compared. The highest torque has been achieved by Iula [40], but the weight of the motor is three times that of the proposed motor. It can therefore be said that the results obtained in the laboratory are far more than acceptable. Also, the results were obtained with lower supply voltage.

## V. CONCLUSION

This paper outlines the development and experimental testing of an ultrasonic multicell piezoelectric motor featuring a multi-rotor structure. The structure was manufactured and validated in a laboratory test bench. Finally, a comparative analysis was conducted between the new multi-rotor structure and the previous MPM prototype. The modular design of the new structure enhances ease of assembly and overall reliability. The speed of the shaft has been significantly increased by using a multi-rotor structure. A direct comparison of the MPM structures is presented in the Tab 3. The efficiency of the MPM with multi-rotors is approximately 15-18%, while the calculated theoretical efficiency is 20%. The previous MPM prototype has an efficiency of less than 10%. Considering the efficiency and total mass of the motors, the power per unit weight is significantly improved. Direct comparison of MPM with multi-rotor and previous MPM power-weight and maximum torque-weight is 15.79 W/kg vs 5.33 W/kg and 0.48 Nm/kg vs 0.23 Nm/kg, respectively. Additionally, it is reasonable to assume that increasing the supply voltage would yield better results. However, certain

aspects require redesigning, such as the shaft connection and gearbox.

The main characteristics of the new MPM were evaluated. Measurements were made and compared with analytical calculations and FEA simulations. The simulated resonant frequency was 22.83 kHz, while the measured frequency was approximately 22.32 kHz. In addition, a maximum shaft speed of 512 rpm was achieved with a voltage of 86 Vrms, and the maximum blocking torque was 120 mNm. The difference in results between calculations and experimental results is aproximately 15% which is an acceptable value for comparing ideal and real model. The efficiency of the MPM with multi-rotors is approximately 14-17%, whereas the calculated theoretical efficiency is 20%.

A trend is emerging towards simplifying the design of piezoelectric motors; however, these motors still have a complex mechanical structure, contributing to enhanced mechanical properties. The integration of three independent actuators with individual rotors has significantly improved both maximum speed and torque output. The optimization of the contact surface between the rotor and stator has resulted in improved operating conditions for the motor.

In contrast to previous MPM structures characterized by punctiform contact surfaces, the novel multi-rotor structure successfully eliminates most of the associated disadvantages. This design shift represents a significant advancement in the pursuit of more efficient and effective piezoelectric motor systems.

## REFERENCES


[1] H. Jin, X. Gao, K. Ren, J. Liu, L. Qiao, M. Liu, W. Chen, Y. He, S. Dong, Z. Xu, and F. Li, "Review on piezoelectric actuators based on high-performance piezoelectric materials," *IEEE Trans. Ultrason., Ferroelectr., Freq. Control*, vol. 69, no. 11, pp. 3057–3069, Nov. 2022.

[2] J. Li, J. Deng, S. Zhang, F. Che, and Y. Liu, "Step displacement improving method of inertial actuated piezoelectric robot based on diagonal deformation trajectory," *IEEE Trans. Ind. Electron.*, vol. 71, no. 4, pp. 3944–3952, Apr. 2024.

[3] G. B. Lucas, B. A. De Castro, J. A. Ardila-Rey, A. Glowacz, J. V. F. Leão, and A. L. Andreoli, "A novel approach applied to transient short-circuit diagnosis in TIMs by piezoelectric sensors, PCA, and wavelet transform," *IEEE Sensors J.*, vol. 23, no. 8, pp. 8899–8908, Apr. 2023.

[4] W. Wang, J. Deng, J. Li, S. Zhang, and Y. Liu, "A small and agile ring-shaped tripodal piezoelectric robot driven by standing and traveling mechanical waves," *IEEE Trans. Ind. Electron.*, vol. 71, no. 3, pp. 2769–2778, Mar. 2023.

[5] Q. Pan, Y. Zhang, X. Chen, Q. Wang, and Q. Huang, "Development of a novel resonant piezoelectric motor using parallel moving gears mechanism," *Mechatronics*, vol. 97, Feb. 2024, Art. no. 103097. [Online]. Available: https://linkinghub.elsevier.com/retrieve/pii/S0957415823001538

[6] D. Xu, X. Zhang, L. Zhao, and S. Yu, "A novel rotary ultrasonic motor using the longitudinal vibration mode," *IEEE Access*, vol. 7, pp. 135650–135655, 2019.

[7] C. Li and C. Lu, "A micro piezoelectric motor with multiple excitation modes and methods," *IEEE Access*, vol. 8, pp. 190981–190988, 2020.

[8] M. Wojtaś, T. J. Bednarchuk, and I. Bdikin, "New hybrid: [H-$\beta$-(4-Pyridyl)-Ala-OH] tetrafluoroborate—Crystal structure and strong piezoelectricity," *CrystEngComm*, vol. 25, no. 25, pp. 3609–3617, 2023. [Online]. Available: https://pubs.rsc.org/en/content/articlehtml/2023/ce/d3ce00308f

[9] I. Jankowska-Sumara, "Phase transitions in $Pb[(Ni_{1/3}Sb_{2/3})_xTi_yZr_z]O_3$ solid solution ceramics studied by piezoelectric measurements," *J. Electroceram.*, vol. 25, nos. 2–4, pp. 168–173, Oct. 2010. [Online]. Available: https://link.springer.com/article/10.1007/s10832-010-9611-x

[10] J. Li, S. Zeng, S. Liu, N. Zhou, and T. Qing, "Tribological properties of textured stator and PTFE-based material in travelling wave ultrasonic motors," *Friction*, vol. 8, no. 2, pp. 301–310, Apr. 2020.

[11] K. Spanner and B. Koc, "Piezoelectric motors, an overview," *Actuators*, vol. 5, no. 1, p. 6, Feb. 2016. [Online]. Available: http://www.mdpi.com/2076-0825/5/1/6

[12] L. Ambroziak, D. Ołdziej, and A. Koszewnik, "Multirotor motor failure detection with piezo sensor," *Sensors*, vol. 23, no. 2, p. 1048, Jan. 2023. [Online]. Available: https://www.mdpi.com/1424-8220/23/2/1048/htm

[13] A. Čeponis, D. Mažeika, P. Vasiljev, and R. Bareikis, "5-DOF cone-shaped piezoelectric positioning robot for optical systems," *Sens. Actuators A, Phys.*, vol. 354, May 2023, Art. no. 114280.

[14] S. Shi, Z. Huang, J. Yang, Y. Liu, W. Chen, and K. Uchino, "Development of a compact ring type MDOF piezoelectric ultrasonic motor for humanoid eyeball orientation system," *Sens. Actuators A, Phys.*, vol. 272, pp. 1–10, Apr. 2018. [Online]. Available: https://linkinghub.elsevier.com/retrieve/pii/S0924424717314723

[15] T. Mashimo and S. Izuhara, "Review: Recent advances in micromotors," *IEEE Access*, vol. 8, pp. 213489–213501, 2020.

[16] Y. Liu, J. Deng, and Q. Su, "Review on multi-degree-of-freedom piezoelectric motion stage," *IEEE Access*, vol. 6, pp. 59986–60004, 2018.

[17] Z. Lyu, Q. Xu, and L. Zhu, "Design of a compliant vertical micropositioning stage based on lamina emergent mechanisms," *IEEE/ASME Trans. Mechatronics*, vol. 28, no. 4, pp. 2131–2141, Aug. 2023.

[18] Y.-H. Chen, L. Wang, J.-M. Jin, and D.-Y. Lai, "Optimization of stator structure of traveling wave hollow ultrasonic motor," in *Proc. 16th Symp. Piezoelectricity, Acoustic Waves, Device Appl. (SPAWDA)*, Oct. 2022, pp. 190–195.

[19] X. Ma, J. Liu, J. Deng, Q. Liu, and Y. Liu, "A rotary traveling wave ultrasonic motor with four groups of nested PZT ceramics: Design and performance evaluation," *IEEE Trans. Ultrason., Ferroelectr., Freq. Control*, vol. 67, no. 7, pp. 1462–1469, Jul. 2020.

[20] S. H. Jahantab, Y. Hojjat, B. G. Namin, and M. Shirkosh, "A novel spherical ultrasonic motor with wire stators and measuring torque and preload via a new method," *Sci. Rep.*, vol. 13, no. 1, pp. 1–13, Jul. 2023. [Online]. Available: https://www.nature.com/articles/s41598-023-39111-8

[21] R. Ryndzionek, M. Michna, M. Ronkowski, and J.-F. Rouchon, "Chosen analysis results of the prototype multicell piezoelectric motor," *IEEE/ASME Trans. Mechatronics*, vol. 23, no. 5, pp. 2178–2185, Oct. 2018.

[22] R. Ryndzionek, L. Sienkiewicz, M. Michna, and F. Kutt, "Design and experiments of a piezoelectric motor using three rotating mode actuators," *Sensors*, vol. 19, no. 23, p. 5184, Nov. 2019. [Online]. Available: https://www.mdpi.com/1424-8220/19/23/5184

[23] R. Ryndzionek, L. Sienkiewicz, M. Michna, and M. Chodnicki, "Design evolution of the ultrasonic piezoelectric motor using three rotating mode actuators," *IEEE Access*, vol. 9, pp. 79416–79423, 2021.

[24] C. Zhao and L. Li, "A method to obtain the repeatability of amplitude sensitivity of a piezoelectric pressure measurement system based on pressure excitation and response measuring points near pulse amplitudes," *IEEE Sensors J.*, vol. 23, no. 24, pp. 30516–30521, Dec. 2023.

[25] Y. Liu, D. Xu, W. Chen, K. Li, and L. Wang, "Design and experimental evaluation of a stepper piezoelectric actuator using bending transducers," *IEEE Access*, vol. 6, pp. 50518–50525, 2018.

[26] B. Hao, L. Wang, R. Wang, Y. Sun, J. Jin, and Q. Xu, "Numerical analysis and experimental investigation on a novel piezoelectric-actuated rail-type mobile platform," *IEEE/ASME Trans. Mechatronics*, vol. 27, no. 2, pp. 744–752, Apr. 2022.

[27] C. Cui, Z. Li, Y. Zhang, and Y. Wang, "Linear piezoelectric motor for topography detector of diamond wire," *IEEE Access*, vol. 7, pp. 166975–166983, 2019.

[28] Y. Zhang, T. Xu, J. Hu, Z. Huang, and Q. Pan, "Resonant-type piezoelectric screw motor for one degree of freedom positioning platform application," *IEEE Access*, vol. 8, pp. 133905–133913, 2020.

[29] K. Murai, D. Kong, H. Tamura, and M. Aoyagi, "Hollow cylindrical linear stator vibrator using a traveling wave of longitudinal axisymmetric vibration mode," *Ultrasonics*, vol. 129, Mar. 2023, Art. no. 106910.

[30] X. Dong, K. Uchino, C. Jiang, L. Jin, Z. Xu, and Y. Yuan, "Electromechanical equivalent circuit model of a piezoelectric disk considering three internal losses," *IEEE Access*, vol. 8, pp. 181848–181854, 2020. [Online]. Available: https://ieeexplore.ieee.org/document/9212357/

[31] B. Ju, Z. Guo, Y. Liu, G. Qian, L. Xu, and G. Li, "Self-sensing vibration suppression of piezoelectric cantilever beam based on improved mirror circuit," *IEEE Access*, vol. 7, pp. 148381–148392, 2019.
[32] Q. Lu, J. Wen, Y. Hu, J. Li, and J. Ma, "An integrated piezoelectric inertial actuator controlled by cam mechanisms," *IEEE Access*, vol. 9, pp. 152756–152764, 2021.
[33] Y. Ting, J.-S. Huang, F.-K. Chuang, and C.-C. Li, "Dynamic analysis and optimal design of a piezoelectric motor," *IEEE Trans. Ultrason., Ferroelectr., Freq. Control*, vol. 50, no. 6, pp. 601–613, Jun. 2003.
[34] M. Budinger, J.-F. Rouchon, and B. Nogarede, "Analytical modeling for the design of a piezoelectric rotating-mode motor," *IEEE/ASME Trans. Mechatronics*, vol. 9, no. 1, pp. 1–9, Mar. 2004.
[35] D. Bai, Q. Quan, D. Tang, and Z. Deng, "Design and experiments of a novel rotary piezoelectric actuator using longitudinal-torsional convertors," *IEEE Access*, vol. 7, pp. 22186–22195, 2019. [Online]. Available: https://ieeexplore.ieee.org/document/8637940/
[36] L. Yang, X. Hu, M. Yang, Y. Huan, W. Ren, Y. Xiong, and H. Li, "A novel traveling wave rotary ultrasonic motor with piezoelectric backup function," *J. Intell. Mater. Syst. Struct.*, vol. 34, no. 20, pp. 2414–2427, Dec. 2023. [Online]. Available: https://journals.sagepub.com/doi/full/10.1177/1045389X231187484
[37] Y. Chen, J. Yang, L. Li, and S. Xiao, "Design and experiments of a new internal cone type traveling wave ultrasonic motor," *Arch. Acoust.*, vol. 48, no. 3, pp. 373–380, 2023. [Online]. Available: https://journals.pan.pl/dlibra/publication/145242/edition/128258/content
[38] J. Leng, L. Jin, X. Dong, H. Zhang, C. Liu, and Z. Xu, "A multi-degree-of-freedom clamping type traveling-wave ultrasonic motor," *Ultrasonics*, vol. 119, Feb. 2022, Art. no. 106621.
[39] X. Lu, Z. Wang, H. Shen, K. Zhao, T. Pan, D. Kong, and J. Twiefel, "A novel dual-rotor ultrasonic motor for underwater propulsion," *Appl. Sci.*, vol. 10, no. 1, p. 31, Dec. 2019. [Online]. Available: https://www.mdpi.com/2076-3417/10/1/31/htm
[40] A. Iula and G. Bollino, "A travelling wave rotary motor driven by three pairs of Langevin transducers," *IEEE Trans. Ultrason., Ferroelectr., Freq. Control*, vol. 59, no. 1, pp. 121–127, Jan. 2012.

**ROLAND RYNDZIONEK** (Senior Member, IEEE) received the M.Sc. degree in electrical engineering from Gdańsk University of Technology (GUT), Gdańsk, Poland, in 2010, the M.Sc. degree in electrical engineering from INP ENSEEIHT, Toulouse, France, in 2012, and the Ph.D. degree in electrical engineering from GUT and INP, in 2015. From 2015 to 2017, he was a Postdoctoral Research Engineer with the SuperGrid Institute, Lyon, France. Since 2017, he has been with GUT, where he is currently an Assistant Professor. His scientific and research interests include development of piezoelectric motors for embedded applications, designing of the mechatronic structures, and power converters.